*MRS Communications (2017)*, *7*, 383–390
© Materials Research Society, 2017
doi:10.1557/mrc.2017.73

MRS Communications

Biomaterials for 3D Cell Biology Prospective Article

# The control of stem cell morphology and differentiation using three-dimensional printed scaffold architecture

**Murat Guvendiren,** Otto H. York Department of Chemical, Biological and Pharmaceutical Engineering, Department of Bioengineering, New Jersey Institute of Technology, University Heights, Newark, NJ 07102, USA; New Jersey Center for Biomaterials, Rutgers University, Piscataway, NJ 08854, USA
**Stephanie Fung** and **Joachim Kohn,** New Jersey Center for Biomaterials, Rutgers University, Piscataway, NJ 08854, USA
**Carmelo De Maria, Francesca Montemurro,** and **Giovanni Vozzi,** Department of Ingegneria dell'Informazione, Research Center "E. Piaggio", University of Pisa, 56100 Pisa, Italy

Address all correspondence to Joachim Kohn at **kohn@rutgers.edu**

(Received 23 May 2017; accepted 10 August 2017)

## Abstract

In this work, we investigated the interactions of human mesenchymal stem cells (hMSCs) with three-dimensional (3D) printed scaffolds displaying different scaffold architectures. Pressure-assisted microsyringe system was used to fabricate scaffolds with square (SQR), hexagonal (HEX), and octagonal (OCT) architectures defined by various degrees of curvatures. OCT represents the highest degree of curvature followed by HEX, and SQR is composed of linear struts without curvature. Scaffolds were fabricated from poly(L-lactic acid) and poly(tyrosol carbonate). We found that hMSCs attached and spread by taking the shape of the individual struts, exhibiting high aspect ratios (ARs) and mean cell area when cultured on OCT scaffolds as compared with those cultured on HEX and SQR scaffolds. In contrast, cells appeared bulkier with low AR on SQR scaffolds. These significant changes in cell morphology directly correlate with the stem cell lineage commitment, such that 80 ± 1% of the hMSCs grown on OCT scaffolds differentiated into osteogenic lineage, compared with 70 ± 4% and 62 ± 2% of those grown on HEX and SQR scaffolds, respectively. Cells on OCT scaffolds also showed 2.5 times more alkaline phosphatase activity compared with cells on SQR scaffolds. This study demonstrates the importance of scaffold design to direct stem cell differentiation, and aids in the development of novel 3D scaffolds for bone regeneration.

## Introduction

Stem cells are an important cell source in tissue engineering and regenerative medicine due to their ability to self-renew, migrate, and differentiate into a wide range of tissue-specific cells, including adipogenic (fat), osteogenic (bone), myogenic (muscle), and chondrogenic (cartilage) cells.[1–6] It is now a well-known fact that that stem cells are responsive to their microenvironment.[7] In this regard, chemical, mechanical, and topographical cues present in the microenvironment influence stem cell behavior, including adhesion, proliferation, migration, and differentiation.[7–13] Recent studies have shown that the topography of the substrate alone regulates differentiation of the stem cells.[14–21]

An induction media condition comprised soluble biologic cues is generally required to drive stem cells toward a certain phenotype in vitro. Thus, it is of great importance to decouple media-induced induction from material-based (chemistry, stiffness, and topography) stimulation.[8] One of the outstanding model culture media systems for stem cells is a 1:1 mixed adipogenic/osteogenic induction media.[16] This model culture system allows investigation of stem cell phenotype decision between adipogenic and osteogenic lineages solely based on material and/or scaffold properties. Adipogenic and osteogenic cells have very distinct morphologies. Adipogenic cells are usually rounded with low spreading, allowing for maximum lipid storage,[5,22] whereas osteogenic cells exhibit higher degrees of cell spreading, which has been shown to promote calcium deposition of osteocytes during bone remodeling.[23] Using this model culture system, Chen and co-workers performed single-cell experiments on surfaces with restricted adhesive regions, and demonstrated that the size and shape of the adhesive regions controlled cellular contractility and differentiation of human mesenchymal stem cells (hMSCs).[16] They showed that cellular spreading due to myosin-generated contractility results in higher levels of Ras homolog gene family member A (RhoA), Rho-associated protein kinase (ROCK), and myosin light chain phosphorylation, leading to osteogenic differentiation.[16] Ruiz and Chen showed the emergence of patterned stem cell differentiation toward adipogenic or osteogenic lineage within multicellular aggregates confined in different geometries.[15] They showed that the contractile activity of the cells could either be hindered or enhanced spatially for the multicellular aggregates based on the surface topography they reside on.[15] Following this study, Mrksich and co-workers demonstrated the effect of curvature on adipogenic and osteogenic differentiation of MSCs on two-dimensional (2D) cell adhesive



https://doi.org/10.1557/mrc.2017.73 Published online by Cambridge University Press

patterns.[24] They demonstrated that contractile cells (residing on the curved regions of flower, star, and holly shapes) display enhanced activation of c-JNK (Jun N-terminal kinase) and ERK (extracellular related kinase) 1/2 with elevated wingless-type (Wnt) signaling promoting osteogenesis.[24] In addition, Guvendiren and Burdick defined a morphological relationship based on cell aspect ratio (AR) and area to predict lineage commitment of hMSCs between adipogenic and osteogenic fate using hydrogel surface wrinkling patterns.[14] They observed that cells with spread areas $<10^3$ μm$^2$ and AR <4 differentiated into adipogenic progenitors, whereas cells outside of this morphological region always differentiated into an osteogenic phenotype.[14] Furthermore, Treiser et al. developed a high content imaging and single-cell modeling approach to forecast lineage commitment of stem cells from very early (24 h) variations in cell shape and cytoskeletal organization.[25] Although these studies have shown the importance of substrate geometry on stem cell behavior, the explored systems are 2D culture systems, and do not necessarily represent the three-dimensional (3D) microenvironment of stem cells. In this regard, Viswanathan el al. used polymerized high internal phase emulsion (polyHIPE) foams with open or closed pore structures with different levels of connectivity as well as pore surface topology in 3D.[26] They demonstrated that the osteogenic differentiation of human mesenchymal progenitor (hES-MP) cells is controlled by the interconnectivity, architecture and surface topology of the foams.[26] However, the effect of curvature in a 3D setting has not yet been studied.

The 3D printing is considered a revolutionary manufacturing technique to fabricate custom-designed, highly complex scaffolds for tissue engineering applications.[27–31] In this work, we took advantage of 3D printing to design and fabricate 3D scaffolds in various shapes, including square, hexagonal, and octagonal, with different curvatures. For this purpose, we chose to use poly(tyrosol carbonate) (PTyC). Tyrosol is readily available from natural resources such as olive oil mill waste waters, and is classified as GRAS (generally recognized as safe) by the FDA (Food and Drug Administration). Kohn and co-workers developed a wide range of tyrosine-derived polycarbonates with tunable properties,[32–34] including a recent group of tyrosine-based polymers with high strength that undergo enzymatic surface erosion.[35] In this study, we investigated stem cell differentiation using a model induction system: osteogenic/adipogenic mixed induction media. We also studied the spatial and overall effect of architecture on stem cell differentiation.

## Materials and methods

### Scaffold design and fabrication

Scaffolds were fabricated from PTyC or poly(L-lactic acid) (PLLA) (Product No: B6002-2; LACTEL Absorbable Polymers, USA). The inks for 3D printing were fabricated by dissolving the polymers in chloroform to obtain 10% (w/v) polymer solution. Pressure-assisted microsyringe system (PAM) was used to fabricate the scaffolds. Among the rapid prototyping methods based on CAD/CAM systems, the PAM technique exploits the pressure-driven extrusion of a polymer solution through a capillary needle and allows the fabrication of 2D and 3D polymeric scaffolds in high resolution. This automated system was developed at the Research Centre 'E. Piaggio' of the University of Pisa.[36]

The deposition unit consists of a stainless-steel syringe equipped with a 5–20 μm glass capillary needle, through which a solution of the chosen polymer, in a volatile solvent, is extruded by the application of filtered compressed air. The unit is able to deposit polymer solutions with a range of viscosity from 10 to 300 cP (mPa.s). An electronically controlled pressure valve is employed to apply a constant pressure in the range 10–300 mmHg to the syringe. A 0.1 μm resolution three-axis micropositioner, designed and built in-house, allows the control of motors in terms of speed and position. The syringe is mounted on the *z*-axis of the motion system, whereas the *x*- and *y*-axis motors are used to move the supporting substrate, usually a glass plate, relative to the syringe position. The entire system, including valves, pressure regulators, sensors, and position controllers, is interfaced to, and controlled by, an IRIS card (Eclipse, Pisa, Italy), which enables the control of motor speed and position. The control software was written in C language: its user-friendly graphic interface allows a variety of patterns with simple or complex topographies to be designed and deposited. The lateral dimensions of the deposited structures are in the range of 5–600 μm, depending on the pressure applied to the syringe, the viscosity of the solution, the motor speed, and the internal diameter of the syringe tip. All these working parameters can be controlled through the user interface. The system has been characterized and optimized and a simple model simulating the fluid dynamics of the deposition process has been developed.[36,37]

Three designs with distinct architectures (square, hexagonal, and octagonal) were used to create the scaffolds. Each scaffold design was composed of three layers with identical designs, the second and the third layer, were shifted by 500 μm with respect to each other. Scaffolds were assembled by depositing a water-soluble polymer spacer (Hydrofilm, Lucart, Italy) between the layers to prevent their collapse. The needle used during the extrusion had a diameter of 150 μm, and the deposition pressure was adjusted to obtain constant line widths of 100 μm.

### Scaffold mechanical tests

Mechanical properties of the scaffolds, including elastic modulus, maximum stress, strain at brake, and toughness, were measured with a uniaxial testing machine (Zwick/Roell mod. Z005, Zwick GmbH & Co. Germany) equipped with a 100 N cell load. Samples were subjected to tensile tests with a constant deformation of 0.05%/s till break.[38,39] To better analyze the mechanical properties of the PTyC and PLLA structures, spin coated films made of the polymers were prepared by spin coating 200 μL of polymer solution of both biomaterials at 1700 rpm for 15 s using a spin-coating system (SUSS Microtech, Switzerland). Statistical analysis was performed as two-way


https://doi.org/10.1557/mrc.2017.73 Published online by Cambridge University Press

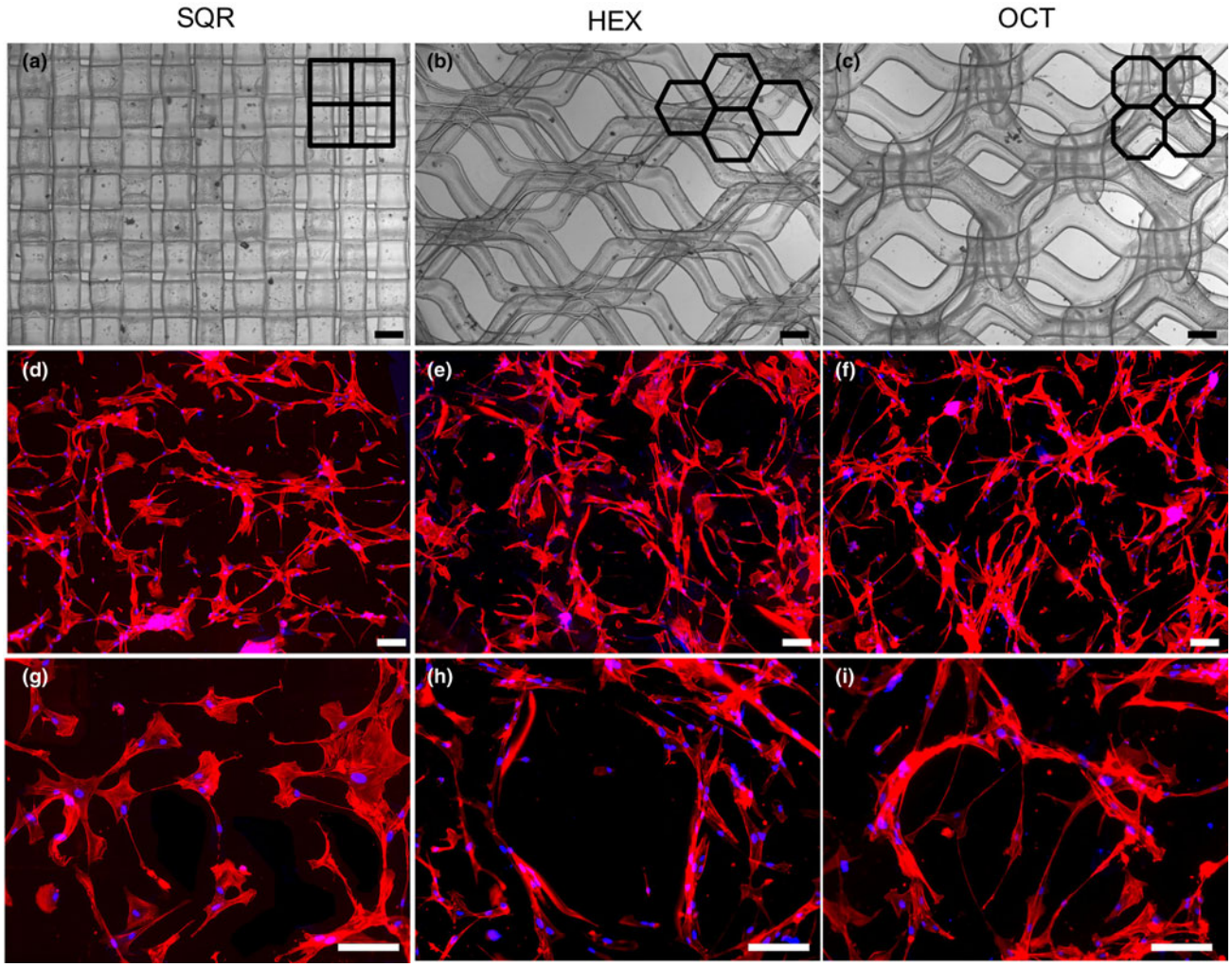



**Figure 1.** (a–c) Phase contrast images of the 3D scaffolds printed from PTyC using square (SQR), hexagon (HEX), and octagon (OCT) architecture. (d–i) Fluorescent images of hMSCs cultured on these scaffolds for 14 days (F-actin in red and cell nuclei in blue). Scale bars for the top two rows are 200 μm and for the bottom row are 100 μm. (Merged images of the phase contrast and fluorescence channels are given in the Supplementary Fig. S2.)

analysis-of-variance (ANOVA) test, comparing cell means regardless of rows and columns with $\alpha = 0.05$.

## Preparation of scaffolds for cell culture

The 3D printed scaffolds were dried under vacuum for 3 days, and immersed in 70% ethanol for 10 min followed by drying overnight. Scaffolds were sterilized under a germicidal UV lamp for 2 h on each side, and immersed in Dulbecco's phosphate-buffered saline (DPBS) in a non-treated tissue culture 24-well plate. Scaffolds were then incubated in fibronectin from bovine plasma (20 μg/mL, Sigma) in DPBS at 37 °C overnight. Scaffolds were washed with DPBS three times, and maintained in growth medium at 37 °C prior to cell seeding. For control studies, scaffolds were incubated in DPBS (without fibronectin) at 37 °C overnight, washed three times with fresh DPBS, and maintained in the growth medium at 37 °C prior to cell seeding.

## Cell culture and reagents

hMSCs isolated from normal adult human bone marrow (donor was 30 years old African American male, Lonza) were expanded in growth media [$\alpha$-MEM (minimum essential medium)], supplemented with 10% FBS (fetal bovine serum, Atlanta Biosciences) and 25 μg/mL gentamicin (Sigma Aldrich). For studies of stem cell spreading and morphology assessment, cells were seeded on the scaffolds and incubated for up to 14 days in growth media. For differentiation studies, after 24 h incubation in the growth medium, cells were cultured in osteogenic/adipogenic mixed media [1:1 osteogenic and adipogenic mixed induction media (R&D Systems Inc.)] for 14 days. Media were refreshed every 3 days.

## Cell activity assays and staining

Cell viability was measured using Alamar Blue assay (Bio-Rad) on culture days 1, 7, and 14. On day 14, cells were washed with



https://doi.org/10.1557/mrc.2017.73 Published online by Cambridge University Press

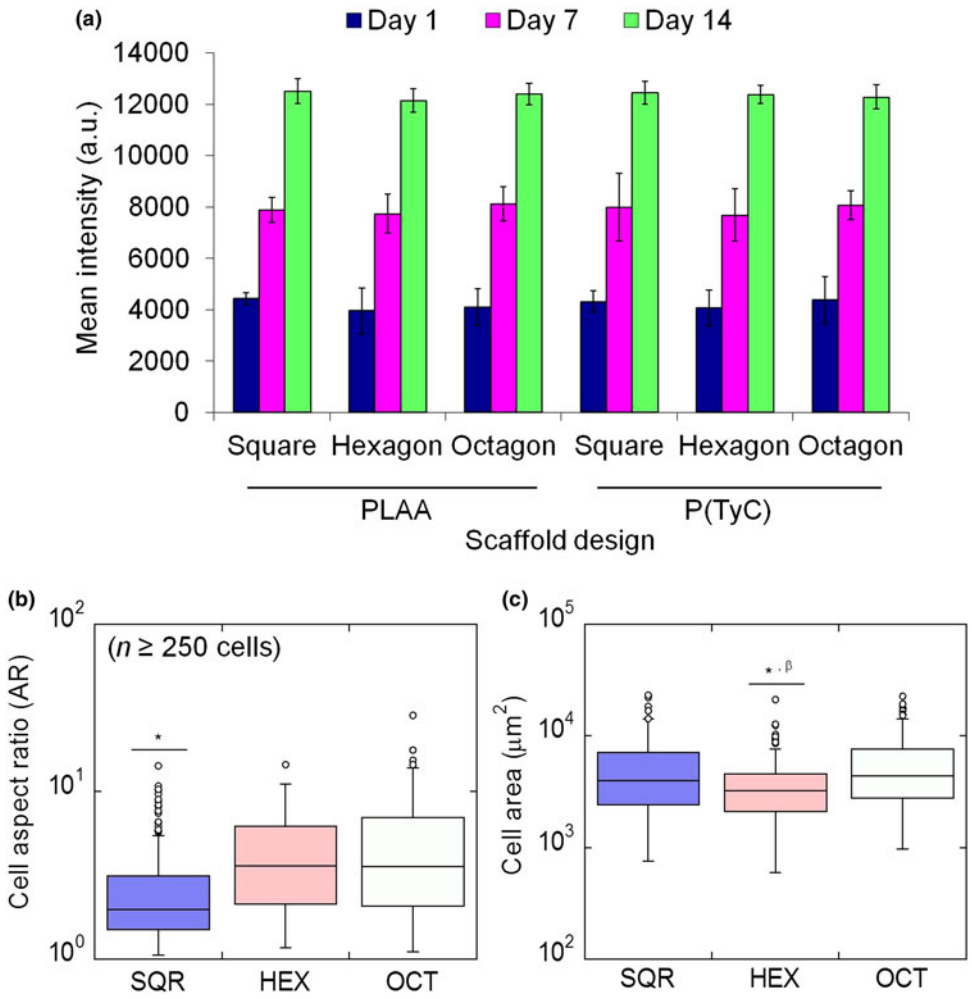



**Figure 2.** (a) Alamar Blue assay results plotted as mean intensity versus scaffold design. Cell aspect ratio (AR) (b) and cell area (c) for hMSCs cultured on PTyC scaffolds with square (SQR), hexagonal (HEX), and octagonal (OCT) architecture plotted using Box-and-Whiskers diagram. For cell AR in (b) $^{*}P < 0.001$ for SQR versus OCT and HEX. For mean cell area in (c), $^{*}P < 0.001$ for HEX versus OCT, and $^{\beta}P < 0.01$ for HEX versus SQR ($n = 250$ cells).

DPBS, fixed in 4% formalin for 15 min, and incubated in Triton X-100 solution (0.25% Triton X-100 in PBS) for 15 min to permeabilize the cell membrane. For immunostaining, cells were rinsed and exposed to blocking solution (10% horse serum in PBS) for 30 min after permeabilization. Samples were then incubated in solutions of primary antibodies in staining solution [3% bovine serum albumin (BSA)—0.1% Tween-20—0.25% Triton X] overnight at 4 °C. Samples were washed thoroughly with BSA solution (3% BSA), and incubated with secondary antibodies in BSA solution. Cells were washed with PBS, and then stained for nuclei using Hoechst.

For morphological assessment, cells were stained for F-actin with rhodamine–phalloidin (Invitrogen), and for nuclei with Hoechst (Sigma-Aldrich). For differentiation studies, cells were either dual immunostained for osteocalcin (OC) and fatty-acid-binding protein 4 (FABP4) or stained for alkaline phosphatase (ALP) with Fast Blue RR/naphthol solution (Sigma). Human OC antibody (monoclonal mouse IgG1, clone 190125, R&D Systems) and human FABP4 antibody (polyclonal goat IgG, R&D Systems) were used with suitable secondary antibodies: goat anti-mouse IgG H&L (Alexa Fluor® 555, Abcam), and donkey anti-goat IgG H&L (Alexafluor® 488, Abcam), respectively.

ALP activity was measured using the Alkaline Phosphatase Activity Fluorometric Assay Kit (Biovision). Samples were lysed in the assay buffer provided with the kit through three freeze–thaw cycles (at −80 and at 37 °C, respectively). dsDNA content for each sample was quantified by PicoGreen dsDNA quantification assay (Thermo Fisher). ALP activity was normalized to dsDNA content and is expressed as relative to samples grown on tissue culture polystyrene or those grown on the 3D printed scaffold with square design (SQR).

## Analysis and statistics

All images were analyzed using NIH ImageJ software. Cell area was measured by manually drawing the cell boundary


https://doi.org/10.1557/mrc.2017.73 Published online by Cambridge University Press

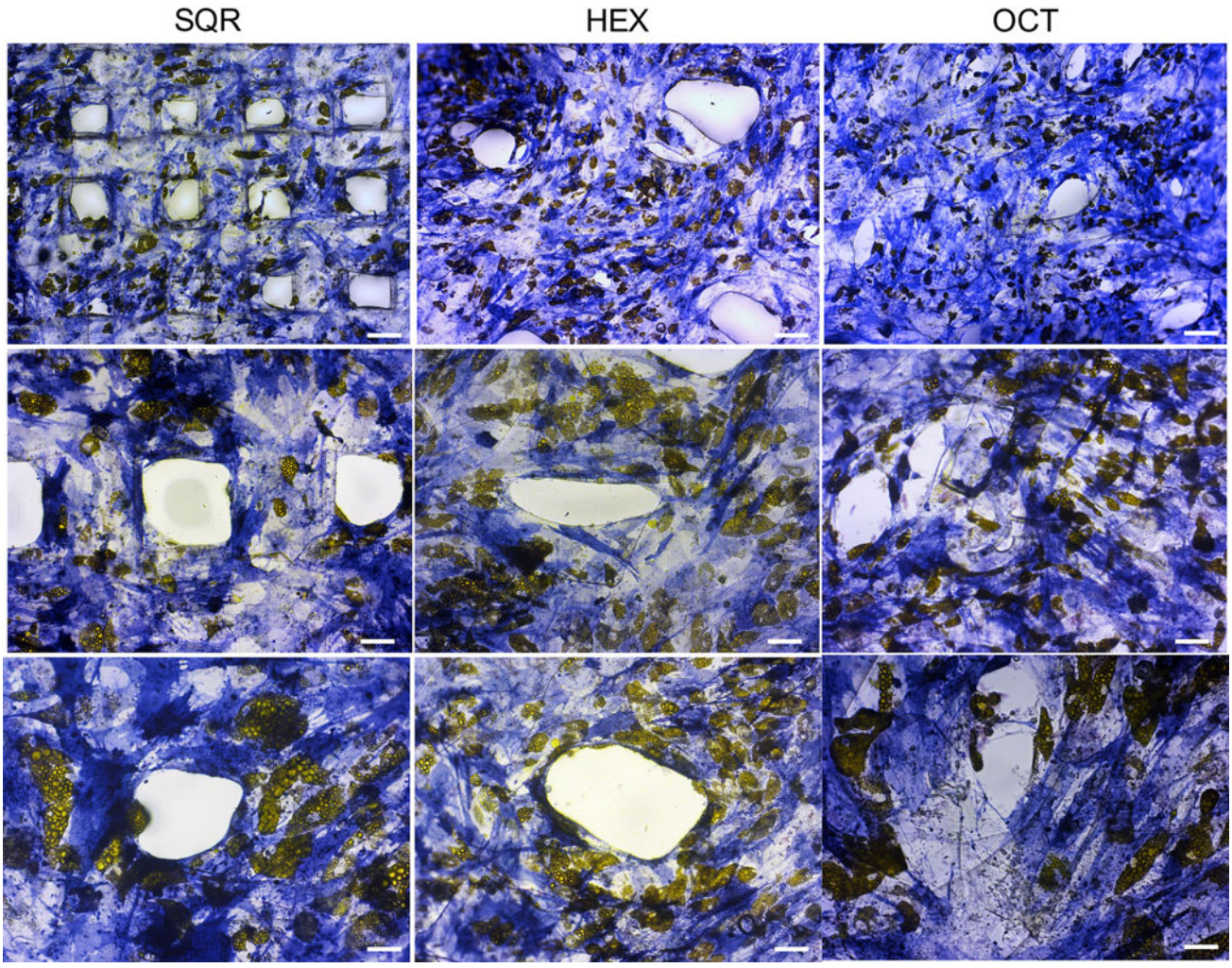



**Figure 3.** Bright field images of hMSCs cultured on scaffolds in mixed osteogenic/adipogenic induction media for 14 days. [blue, Alkaline phosphatase indicating osteogenic (BONE) cells; yellow, Lipid droplets for adipogenic (FAT) cells.]. Scale bars are 200, 100, 50 μm, from top to bottom row, respectively.

and using measure tool. This also gave the AR of the cell (the ratio of major-to-minor axes). Statistical analysis was performed using KleidaGraph (Synergy Software, Reading, PA). All values were presented as mean ± standard deviation of the mean (for $n \geq 3$). ANOVA with Tukey's HSD post hoc test was performed among the groups, with significance defined as confidence level of 0.05.

## Results and discussion

A PAM system was used to fabricate the scaffolds layer-by-layer from PTyC or PLLA. To investigate the effect of curvature on stem cell morphology, spreading, and differentiation, we focused on square (SQR), hexagonal (HEX), and octagonal (OCT) patterns [Figs. 1(a)–1(c)]. First, we characterize the mechanical properties of the scaffolds (Supplementary Fig. S1). The elastic modulus of the PTyC films (107 ± 14 MPa) was approximately two times larger than that of the PLLA films (46 ± 2 MPa). When scaffold architectures are considered, the moduli of SQR (PTyC = 50 ± 14 and PLLA = 25 ± 3 MPa) and HEX (PTyC = 43 ± 7 and PLLA = 21 ± 3 MPa) scaffolds were significantly higher than the OCT (PTyC = 11 ± 7 and PLLA = 18 ± 8 MPa) scaffolds. Here, we would like to note that the modulus values are well above the corresponding modulus values for fat tissue (~3 kPa) and pre-calcified bone (~30–40 kPa),[1,14] thus not a determining factor in our studies. Our results show that the architecture of the scaffold controls the overall stiffness of the scaffold. However, the overall scaffold stiffness values for different designs are not necessarily important for stem cell differentiation as cells initially reside on individual struts, and the stiffness they feel is the stiffness of the polymer rather than stiffness of the overall scaffold.

Our initial studies indicated poor cell adhesion and a lack of uniform cell distribution on our scaffolds even after 14-day culture for both PTyC and PLLA scaffolds. Thus, the scaffolds were incubated in a fibronectin solution, which enhanced stem cell adhesion and ensured uniform distribution of cells [Figs. 1



https://doi.org/10.1557/mrc.2017.73 Published online by Cambridge University Press

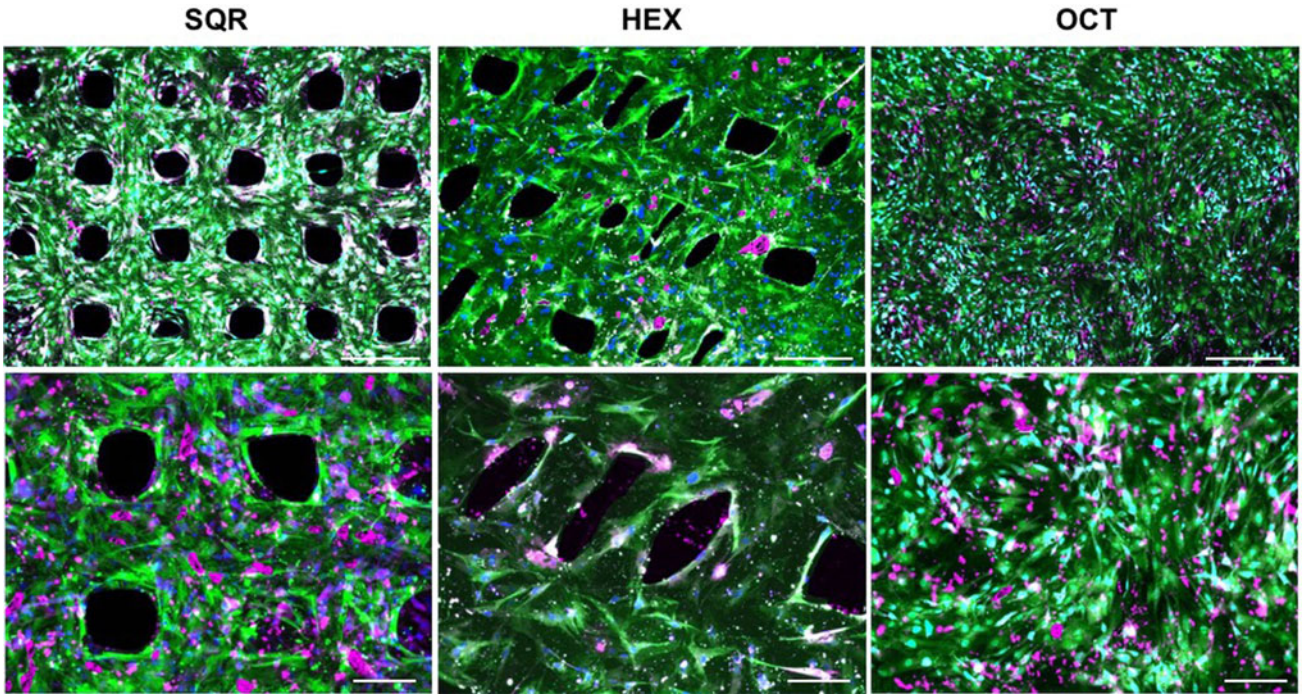



**Figure 4.** Fluorescent images of the dual-immunostained hMSCs cultured on scaffolds in mixed osteogenic/adipogenic induction media for 14 days [green, Osteocalcin indicating osteogenic (BONE) cells; magenta, FABP4 showing lipid droplets in adipogenic (FAT) cells]. Scale bars are 500 and 200 μm, for top and bottom rows, respectively.

(d)–1(i) and Supplementary Fig. S2]. Alamar Blue assay results indicated an increase in metabolic activity with culture time for both PLLA and PTyC scaffolds [Fig. 2(a)]. Stem cells attached and remained viable over time independent of the scaffold architecture and the polymer system. When the scaffolds with identical designs are compared, we did not observe any significant difference in cell morphology and spreading between PLLA and PTyC scaffolds (Supplementary Fig. S3). However, we observed significant differences in cell AR and cell area between scaffold designs [Figs. 2(b) and 2(c)]. We focused on PTyC scaffolds for the remainder of the study as we did not observe any difference between PTyC and PLLA.

hMSCs were found to attach and spread on the scaffolds by aligning themselves along the printed struts [Figs. 1(g)–1(i)]. Stem cells were highly elongated with significantly higher AR for OCT (AR ~ 5.0) and HEX (AR ~ 4.4) as compared with SQR (AR ~ 2.5) scaffolds [Fig. 2(b)]. When cell spreading (defined by mean cell area) was considered [Fig. 2(c)], stem cells on SQR (mean cell area of 5100 $\mu m^2$) and OCT (mean cell area of 5700 $\mu m^2$) scaffolds had significantly higher cell spreading than that of HEX (mean cell area of 3900 $\mu m^2$) scaffolds.

We examined whether these significant changes in cell morphology correlated with differentiation state. Here we would like to note that our study focuses on micro-scale surface patterns and curvature, which requires the use of induction media to evaluate the stem cell fate decision as shown in the literature. In contrast, nano-scale surface patterns are known to induce osteogenic differentiation of stem cells even in the absence of induction media.[40] For this purpose, hMSCs were seeded on 3D printed PTyC scaffolds with SQR, HEX, or OCT patterns. Stem cells were allowed to attach and spread for 1 day in growth media. The media were then replaced with 1:1 adipogenic/osteogenic mixed induction media, and the cells were incubated for 14 days. The cells were stained for ALP as a marker of osteogenesis (Fig. 3). Note that the adipogenic cells appeared yellow after ALP staining due to oil droplets. Qualitatively, the majority of the cells stained positive for ALP.

Another sample group was dual-immunostained for OC as a marker of osteogenesis and FABP4 as a marker of adipogenesis (Fig. 4). Due to the selection of secondary antibodies, OC-positive cells appeared green, whereas FABP4-positive cells appeared red under fluorescent microscope. When all cells were quantified, osteogenic differentiation was found to be upregulated (Fig. 5(a)) such that 62 ± 2% of the cells stained positive for OC for SQR scaffolds, followed by 70% ± 4 for HEX scaffolds, and 80 ± 1% for OCT scaffolds (we did not observe any dual-stained cells). ALP activity was also measured as a quantitative measure of osteogenic differentiation. Our analysis showed that the ALP activity followed a similar trend (Fig. 5(b)). The ALP activity of the cells on OCT scaffolds (relative to SQR scaffolds) was significantly higher than that of HEX (1.3 times) and SQR (2.2 times).


https://doi.org/10.1557/mrc.2017.73 Published online by Cambridge University Press

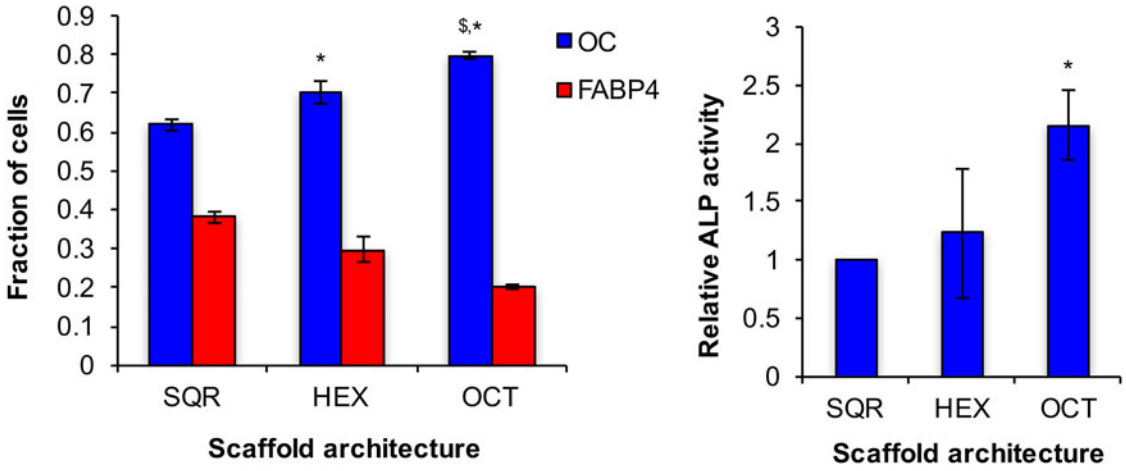



**Figure 5.** (a) Quantitative analysis of immunostaining results showing fraction of cells stained positive for OC (bone) and FABP4 (fat). (b) ALP activity of hMSCs for scaffolds plotted relative to SQR (where relative ALP activity for SQR is set to 1). Relative ALP activity denotes mU ALP/μg DNA (normalized to SQR).

## Conclusion

In summary, we used 3D printed scaffolds to investigate the effects of scaffold architecture on stem cell differentiation. The scaffolds were printed using PLLA or PTyC. We did not observe any significant differences between scaffolds fabricated from PLLA or PTyC in terms of stem cell attachment, morphology, and viability. However, we observed significant differences in stem cell spreading and AR as well as lineage commitment dependent on scaffold architecture. When stem cell morphology is considered, the following relationships were obtained: OCT > HEX ≫ SQR, for cell AR, and OCT ≥ SQR ≫ HEX, for mean cell area. Cells displayed the largest AR and cell area on OCT scaffolds compared those grown on other scaffolds. We believe that this is due to the highly curved surfaces displayed by the OCT scaffolds. Cells were elongated on HEX scaffolds, yet had the lowest mean cell area. On SQR scaffolds, cells were bulkier with low AR, but had high cell area. We observed significantly higher ALP activity and OC staining for hMSCs cultured on OCT scaffolds after 14 days of culture in the mixed induction media. Our results suggest that OCT architecture (with abundance of curved surfaces) is more efficient to drive stem cells into osteogenic lineage. Our study demonstrated the importance of scaffold architecture, which may be an important factor in the design of bone scaffolds.

## Supplementary material

The supplementary material for this article can be found at https://doi.org/10.1557/mrc.2017.73.

## Acknowledgments

Authors would like to thank Tyler Hoffman for his assistance on cell culture assays. This study was supported by RESBIO, the "Resource for polymeric biomaterials", funded by the National Institute of Health, National Institute of Biomedical Imaging and Bioengineering Award Number P41EB001046, and by the National Science Foundation under Grant No. 1714882.

## References

1. A.J. Engler, S. Sen, H.L. Sweeney, and D.E. Discher: Matrix elasticity directs stem cell lineage specification. *Cell* **126**, 677 (2006).
2. T.S. Stappenbeck and H. Miyoshi: The role of stromal stem cells in tissue regeneration and wound repair. *Science* **324**, 1666 (2009).
3. M. Sasaki, R. Abe, Y. Fujita, S. Ando, D. Inokuma, and H. Shimizu: Mesenchymal stem cells are recruited into wounded skin and contribute to wound repair by transdifferentiation into multiple skin cell type. *J. Immunol.* **180**, 2581 (2008).
4. M.F. Pittenger, A.M. Mackay, S.C. Beck, R.K. Jaiswal, R. Douglas, J. D. Mosca, M.A. Moorman, D.W. Simonetti, S. Craig, and D.R. Marshak: Multilineage potential of adult human mesenchymal stem cells. *Science* **284**, 143 (1999).
5. A.E. Grigoriadis, J.N.M. Heersche, and J.E. Aubin: Differentiation of muscle, fat, cartilage, and bone from progenitor cells present in a bone-derived clonal cell population: effect of dexamethasone. *J. Cell Biol.* **106**, 2139 (1988).
6. M. Guvendiren and J.A. Burdick: Stiffening hydrogels to probe short-and long-term cellular responses to dynamic mechanics. *Nat. Commun.* **3**, 792 (2012).
7. J.A. Burdick and G. Vunjak-Novakovic: Engineered microenvironments for controlled stem cell differentiation. *Tissue Eng. A* **15**, 205 (2009).
8. R.A. Marklein and J.A. Burdick: Controlling stem cell fate with material design. *Adv. Mater.* **22**, 175 (2010).
9. D.E. Discher, D.J. Mooney, and P.W. Zandstra: Growth factors, matrices, and forces combine and control stem cells. *Science* **324**, 1673 (2009).
10. D.E. Discher, P. Janmey, and Y.L. Wang: Tissue cells feel and respond to the stiffness of their substrate. *Science* **310**, 1139 (2005).
11. B.G. Keselowsky, D.M. Collard, and A.J. García: Integrin binding specificity regulates biomaterial surface chemistry effects on cell differentiation. *Proc. Natl. Acad. Sci. U. S. A.* **102**, 5953 (2005).
12. A.J. García, M.D. Vega, and D. Boettiger: Modulation of cell proliferation and differentiation through substrate- dependent changes in fibronectin conformation. *Mol. Biol. Cell* **10**, 785 (1999).
13. W.G. Brodbeck, M.S. Shive, E. Colton, Y. Nakayama, T. Matsuda, and J. M. Anderson: Influence of biomaterial surface chemistry on the apoptosis of adherent cells. *J. Biomed. Mater. Res.* **55**, 661 (2001).



https://doi.org/10.1557/mrc.2017.73 Published online by Cambridge University Press

14. M. Guvendiren and J.A. Burdick: The control of stem cell morphology and differentiation by hydrogel surface wrinkles. *Biomaterials* **31**, 6511 (2010).
15. S.A. Ruiz and C.S. Chen: Emergence of patterned stem cell differentiation within multicellular structures. *Stem Cells* **26**, 2921 (2008).
16. R. McBeath, D.M. Pirone, C.M. Nelson, K. Bhadriraju, and C.S. Chen: Cell shape, cytoskeletal tension, and RhoA regulate stem cell lineage commitment. *Dev. Cell* **6**, 483 (2004).
17. C.H. Thomas, J.H. Collier, C.S. Sfeir, and K.E. Healy: Engineering gene expression and protein synthesis by modulation of nuclear shape. *Proc. Natl. Acad. Sci. U. S. A.* **99**, 1972 (2002).
18. A.I. Teixeira, G.A. Abrams, P.J. Bertics, C.J. Murphy, and P.F. Nealey: Epithelial contact guidance on well-defined micro- and nanostructured substrates. *J. Cell Sci.* **116**, 1881 (2003).
19. S. Oh, K.S. Brammer, Y.S.J. Li, D. Teng, A.J. Engler, S. Chien, and S. Jin: Stem cell fate dictated solely by altered nanotube dimension. *Proc. Natl. Acad. Sci. U. S. A.* **106**, 2130 (2009).
20. R.G. Flemming, C.J. Murphy, G.A. Abrams, S.L. Goodman, and P. F. Nealey: Effects of synthetic micro- and nano-structured surfaces on cell behavior. *Biomaterials* **20**, 573 (1999).
21. M. Guvendiren and J.A. Burdick: Engineering synthetic hydrogel microenvironments to instruct stem cells. *Curr. Opin. Biotechnol.* **24**, 841 (2013).
22. F.M. Gregoire, C.M. Smas, and H.S. Sul: Understanding adipocyte differentiation. *Physiol. Rev.* **78**, 783 (1998).
23. V.I. Sikavitsas, J.S. Temenoff, and A.G. Mikos: Biomaterials and bone mechanotransduction. *Biomaterials* **22**, 2581 (2001).
24. K.A. Kilian, B. Bugarija, B.T. Lahn, and M. Mrksich: Geometric cues for directing the differentiation of mesenchymal stem cells. *Proc. Natl. Acad. Sci. U. S. A.* **107**, 4872 (2010).
25. M.D. Treiser, E.H. Yang, S. Gordonov, D.M. Cohen, I.P. Androulakis, J. Kohn, C.S. Chen, and P.V. Moghe: Cytoskeleton-based forecasting of stem cell lineage fates. *Proc. Natl Acad. Sci. U. S. A.* **107**, 610 (2010).
26. P. Viswanathan, M.G. Ondeck, S. Chirasatitsin, K. Ngamkham, G.C. Reilly, A.J. Engler, and G. Battaglia: 3D surface topology guides stem cell adhesion and differentiation. *Biomaterials* **52**, 140 (2015).
27. M. Guvendiren, J. Molde, R.M.D. Soares, and J. Kohn: Designing biomaterials for 3D printing. *ACS Biomater. Sci. Eng.* **2**, 1679 (2016).
28. S. Ji and M. Guvendiren: Recent advances in bioink design for 3D bioprinting of tissues and organs. *Front. Bioeng. Biotechnol.* **5**, 23 (2017).
29. S. Bose, S. Vahabzadeh, and A. Bandyopadhyay: Bone tissue engineering using 3D printing. *Mater. Today* **16**, 496 (2013).
30. S.J. Hollister: Porous scaffold design for tissue engineering. *Nat. Mater.* **4**, 518 (2005).
31. G. Jürgen, B. Thomas, B. Torsten, A.B. Jason, C. Dong-Woo, D.D. Paul, D. Brian, F. Gabor, L. Qing, A.M. Vladimir, M. Lorenzo, N. Makoto, S. Wenmiao, T. Shoji, V. Giovanni, B.F.W. Tim, X. Tao, J.Y. James, and M. Jos: Biofabrication: reappraising the definition of an evolving field. *Biofabrication* **8**, 013001 (2016).
32. V. Tangpasuthadol, S.M. Pendharkar, and J. Kohn: Hydrolytic degradation of tyrosine-derived polycarbonates, a class of new biomaterials. Part I: study of model compounds. *Biomaterials* **21**, 2371 (2000).
33. V. Tangpasuthadol, S.M. Pendharkar, R.C. Peterson, and J. Kohn: Hydrolytic degradation of tyrosine-derived polycarbonates, a class of new biomaterials. Part II: 3-yr study of polymeric devices. *Biomaterials* **21**, 2379 (2000).
34. S.I. Ertel and J. Kohn: Evaluation of a series of tyrosine-derived polycarbonates as degradable biomaterials. *J. Biomed. Mater. Res.* **28**, 919 (1994).
35. S.D. Sommerfeld, Z. Zhang, M.C. Costache, S.L. Vega, and J. Kohn: Enzymatic surface erosion of high tensile strength polycarbonates based on natural phenols. *Biomacromolecules* **15**, 830 (2014).
36. G. Vozzi, A. Previti, D. De Rossi, and A. Ahluwalia: Microsyringe-based deposition of two-dimensional and three-dimensional polymer scaffolds with a well-defined geometry for application to tissue engineering. *Tissue Eng.* **8**, 1089 (2002).
37. M. Mariani, F. Rosatini, G. Vozzi, A. Previti, and A. Ahluwalia: Characterization of tissue-engineered scaffolds microfabricated with PAM. *Tissue Eng.* **12**, 547 (2006).
38. G. Criscenti, C. De Maria, E. Sebastiani, M. Tei, G. Placella, A. Speziali, G. Vozzi and G. Cerulli: Material and structural tensile properties of the human medial patello-femoral ligament. *J. Mech. Behav. Biomed. Mater.* **54**, 141 (2016).
39. M. Mattioli-Belmonte, C. De Maria, C. Vitale-Brovarone, F. Baino, M. Dicarlo, and G. Vozzi: Pressure-activated microsyringe (PAM) fabrication of bioactive glass–poly (lactic-co-glycolic acid) composite scaffolds for bone tissue regeneration. *J. Tissue Eng. Regen. Med.* **11**, 1986 (2015).
40. S. Dobbenga, L.E. Fratila-Apachitei, and A.A. Zadpoor: Nanopattern-induced osteogenic differentiation of stem cells—a systematic review. *Acta Biomater.* **46**, 3 (2016).


https://doi.org/10.1557/mrc.2017.73 Published online by Cambridge University Press